

Research Paper

# Controlling the Basal Texture for Significant Improvements in Mechanical Properties of AZ91D Mg Sheets Using Elevated-Temperature Constrained Groove Pressing

S. Ghorbanhosseini<sup>1\*</sup>, F. Fereshteh-Saniee<sup>1</sup>, A. Sonboli<sup>2</sup>

<sup>1</sup> Department of Mechanical Engineering, Faculty of Engineering, Bu-Ali Sina University, Hamedan, 6517838695, Iran

<sup>2</sup> Department of Materials Engineering and Metallurgy, Faculty of Engineering, Arak University, Arak, 3815688349, Iran

Received 21 December 2024; Received in revised form 27 January 2025; Accepted 23 February 2025

## ABSTRACT

A severe plastic deformation (SPD) technique, namely constrained groove pressing (CGP), is employed to investigate its influence on the texture and mechanical properties of AZ91D magnesium sheets. Three cycles of CGP process were conducted on the AZ91D annealed sheets at elevated temperature. Optical microscopy, scanning electron microscopy, and X-ray diffraction (XRD) were used to characterize microstructural evolutions. Hardness and tensile tests at room temperature were performed to determine the mechanical properties. The microscopy observations showed that  $\beta$ - $Mg_{17}Al_{12}$  particles existed in the annealed sample. The average grain size (AGS) was reduced from 18  $\mu m$  to 14  $\mu m$  after the first CGP cycle. Also, the basal texture of the annealed sample was controlled during the first CGP cycle. The yield strength and elongation of the annealed sheet (129.4 MPa, 24.5%) were respectively increased to 166.7 MPa and 36.1%, by performing just the first pass of the CGP operation. The inverse pole figures showed that the main texture direction was  $[0\ 0\ 0\ 1] \parallel TD$ . Afterward, it was found that 3-passed worksheet had the lowest homogeneity with a maximum inhomogeneity factor of 5.69.

**Keywords:** AZ91D Magnesium alloy; Constrained groove pressing; Microstructure; Texture; Mechanical Properties.

\*Corresponding author. Tel.: +98 912 755 8009.  
E-mail address: s.ghorbanhosseini@basu.ac.ir (S. Ghorbanhosseini)

## 1 INTRODUCTION

THE need for decreasing weights of vehicles, such as those found in the aircraft and automotive industries, and its consequence on lowering the fuel consumption has incited the researchers to develop different Mg-based alloys with a low density, namely  $1.74 \text{ g/cm}^3$ , and a high strength/weight ratio [1-5]. AZ91D is one of the most famous Mg alloys due to its high strength/weight ratio and high corrosion resistance. In the normal condition of solidification, microstructure of AZ91 alloy possesses a dendritic form in which brittle  $\beta\text{-Mg}_{17}\text{Al}_{12}$  phase exists between dendrite arms [6]. The severe plastic deformation (SPD) is a forming technique in which a fine-grained component is produced by inducing high strains into the material without changing the main dimensions of the workpiece [7]. The microstructure of the workpiece is considerably modified during a severe plastic deformation such that the grain size can meaningfully be reduced and, consequently, the mechanical properties of the material would significantly improve, whereas the size of the component is unchanged. This type of strengthening is carried out without addition of alloying elements and/or ceramic particles [8]. During past two decades, various SPD methods have been proposed by different researchers, among which the constrained groove pressing (CGP) technique was introduced for increasing the strength of the sheet metals [9]. A CGP operation is based on repeated corrugating and flattening of a sheet. Combination of shearing, compressing and bending forces are applied to the workpiece through repeated pressing by means of two sets of grooved and flat dies. This operation is schematically illustrated in Fig. 1. In the first stage of a CGP cycle or pass, the workpiece is first corrugated by means of a grooved die (Figs. 1a and 1b). Afterward, in stage 2, by pressing the deformed part between two flat dies, it is plastically deformed into its initial shape (Fig. 1c). Then, the sheet is rotated  $180^\circ$  about its normal axis, and finally, during stages 3 and 4, the corrugating and straightening operations are repeated, respectively (Figs. 1d to 1f). Following this procedure and performing all these 4 stages on a workpiece, one complete pass of the CGP operation is conducted. Redoing the forming cycle shown in Fig. 1 several times, one can induce huge strains into the material, resulting in significant modifications in its microstructure and considerable improvements in its mechanical properties. The main advantage of the CGP process is its applicability to sheet metals.

Hajizadeh et al. [14] increased the microhardness and the yield strength of 1050 Al alloy, namely 62% and 95% respectively, by carrying out four CGP cycles. Lin et al. [15] employed CGP process for producing UFG AZ31 Mg sheets at elevated temperatures. The mechanical and electrical properties together with the corrosion resistance of Al-Mn-Si alloy, deformed through the constrained groove pressing, were also investigated by Pouraliakbar et al. [16]. Moradpour et al. [17] used CGP as an SPD method to produce an Al-Mg alloy (AA 5052) with ultra-fine grains. They discussed the cellular structure formation, precipitates morphology and dynamic strain aging behavior of sheets produced through different CGP passes to interpret tensile properties along rolling (RD) and transverse directions (TD) of the deformed parts in terms of anisotropy. Nazari et al. [18] also investigated the effect of stress relief annealing on mechanical properties, microstructure, and residual stresses of pure copper sheets deformed by CGP technique. They found that stress relief annealing reduced the mean grain size during the first pass but increased its value in the subsequent passes, causing a decrease in mechanical properties. Mozafari et al. [19] examined the wear behavior of Al-Mg sheets produced by CGP technique and compared the findings against those of the annealed coarse-grained alloy. They observed the worn surfaces by using FE-SEM and concluded that the mechanism of wear changed from sticking to plastic deformation band. Evolution of microstructure and superplasticity of an extruded Mg-2wt% Gd sheet after the CGP operation were also studied by Hoseini-Athar et al. [20]. They claimed that, for the fine-grained workpieces subjected to 4 cycles of CGP, the dominant deformation mechanism in the superplastic regime was grain boundary sliding (GBS) controlled by grain boundary diffusion. Wang et al. [21] investigated the influence of lubrication and strain path on the CGPed Aluminum worksheets. They found that the elongation to failure of the produced sheets was improved by employing both the lubricants (Teflon layers and MoS<sub>2</sub> lubricant) while the strength was much lower when just Teflon layers were used; even compared with the sheet processed via an original four-pass parallel-CGP with MoS<sub>2</sub> as lubricant. Ghorbanhosseini and Fereshteh-Saniee [22] optimized the geometrical parameters of CGP grooved dies in order to induce more plastic strain to the Al sheets and reduce the inhomogeneity of the samples. Ghorbanhosseini et al. [23] developed a new fiber texture including components such as  $\{016\} \langle 410 \rangle$ ,  $\{017\} \langle 110 \rangle$ ,  $\{118\} \langle 120 \rangle$  and  $\{106\} \langle 010 \rangle$  by performing up to three cycles constrained groove pressing on the Al 2024 alloy sheets at elevated temperature. They claimed that the significant elongation of 3-passed worksheet (41%) in their study was related to this new fiber texture. Karademir et al. [24] studied the effect of CGP, severe shot peening (SSP) and ultrasonic nanocrystal surface modification (UNSM) on the microstructural evolution of S500MC automotive steels. The results showed that the SSP and UNSM could produce a nanocrystallization layer up to 50-100 micrometer far from the outmost surface. Moreover, the sample strength increased from the 1st pass to 4th pass of CGP; however, the elongation percentage

decreased. Keyvani et al. [25] studied the microstructural evolution and electrochemical properties of ultra-fine grained (UFG) pure copper sheets produced by CGP operation. They found that the CGP process could positively affect the passive behavior of pure copper in the electrochemical field. Moreover, by conducting subsequent CGP cycles the corrosion current density would decrease. Bhardwaj et al. [26] investigated the influence of CGP on the hardening behavior of Ti6Al4V alloy sheets at elevated temperature. Their analyses demonstrated that microstructural evolution occurred due to dynamic recrystallization (DRX) in specimens CGPed at 750 °C whereas work hardening and grain fragmentation was observed in samples CGPed at 550 °C. Wang et al. [27] concentrated on the effect of strain path on different behaviors of AZ31 Mg alloy worksheets processed by CGP. They conducted CGP process on AZ91D sheets at 523 K in three different manners, namely, traditional CGP, 180° cross-CGP and 90° cross-CGP. The superior reduction in the average grain size (AGS) was obtained for traditionally CGPed specimens. Nazari et al. [28] investigated the effects of multi-cut contour method and friction coefficient on the residual stresses of CGPed worksheets. Their results revealed that the residual stresses after the 1st pass of the CGP operation were compressive and they varied to tensile mode by approaching to the thickness center. Fereshteh-Saniee et al. [29] compared the effects of elevated temperature CGP on two different lightweight alloys, namely Al 2024 and Mg AZ91. They also simulated the damage behavior of CGPed Al2024-T3 sheets. Their results showed that the CGP process could not be performed at room temperature for wrought lightweight alloy such as Al2024-T3. Thus, performing CGP process for these alloys should be done at elevated temperature [43]. Bhardwaj et al. [44] studied the Ti64 alloy behavior under CGP process based on various speed. They found that by increasing the pressing speed, some mechanical properties such as yield strength, ultimate tensile strength, and microhardness were improved. Sawalkar & Field [45] developed a new form of pressing for achieving more homogenous copper worksheet during CGP process. Also, they verified their experimental results by analytical and numerical solutions. Farajollahi et al. [46] improved wear behavior of 304L stainless steel under CGP. Their results showed that the hardness and wear resistance were enhanced by conducting more CGP cycles.

The basal texture of Mg alloys that results in low ductility for these alloys, has been considered as an important issue in the field of forming of these alloys. Moreover, among previous researches, there is no report on the basal texture control of constrained groove pressing for AZ91D alloy at elevated temperatures. In this paper, the effect of elevated temperature CGP on the microstructural characterizations and textural evolutions during deformation has been examined by using optical microscopy (OM), scanning electron microscopy (SEM) and X-ray diffraction (XRD). Finally, the mechanical properties of the AZ91D sheets subjected to three cycles of the CGP operation were studied. Controlling the basal texture (i.e. preventing the basal texture growth) of AZ91D Mg alloy can be introduced as a main goal for this research work.

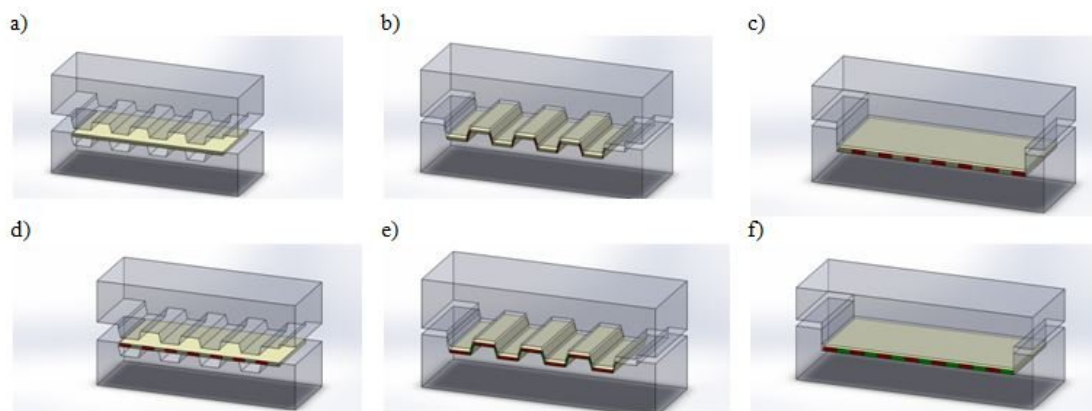


**Fig. 1**  
Various steps for CGP process.

## 2 EXPERIMENTAL PROCEDURES

The CGP process was performed on sheets made of AZ91D Mg alloy (Mg-8.74Al-0.80Zn-0.35Mn in wt %) and with the length/width/thickness of 100/100/2 mm dimensions. The samples were annealed at 350 °C for 2 hours, in an inert argon gas atmosphere, and cooled in the electric furnace. The CGP dies were made of AISI 4140 hot-work tool steel. Three 500-watt electrical heating elements were inserted in each CGP die (Fig. 2). These electrical elements increased the temperature up to 300 °C for performing the CGP tests. A servo electrical press with the capacity of 40 Ton was used to carry out the CGP experiments.

In this article, RD represent the rolling direction, TD represent the transverse direction and ND, represent the normal direction on each worksheet (Fig. 2). For microstructural studies, the sample obtained after each pass was cut in the TD-ND plane. Afterwards, metallography procedures were performed to provide a completely sharp surface based on ASTM E3-11 standard [30]. Different specimens were then smeared in an etchant solution containing 4.26 gr., picric acid, 10 ml acetic acid, 10 ml distilled H<sub>2</sub>O and 150 ml ethanol. Microstructures of various CGPed samples were prepared by employing a UNION 7759 optical microscope (OM) and scanning electron microscopy (SEM) (FEI/Quanta model) equipped with energy dispersive spectroscopy (EDS).

The macrotexture was measured on the RD-TD plane of each sample by X-ray diffraction (XRD). The texture was determined using a PANalytical X-ray diffractometer, which employed Cr K $\alpha$  radiation up to a tilt angle of 75°. For calculating the orientation distribution functions (ODFs), and preparation of the inverse pole figures (IPFs), two incomplete pole figures (PFs) including {0002} and {10 $\bar{1}$ 0} were produced by using the TexTools software (ResMat Co.).

The sub-size tensile test specimens were prepared parallel to RD, based on suggestions made by Xing et al. [31] and with the gauge width and length of 3.0 and 4.0 mm, respectively. A STM-50 testing machine was utilized to conduct the tensile tests at the room temperature.

Finally, the hardness of different samples was measured using a Buehler hardness tester in the TD direction for five points, aparting 10 mm from each other. These hardness tests were performed by exerting a 100 gr., force for 20 sec., using a pyramid with an apex angle of 136°.

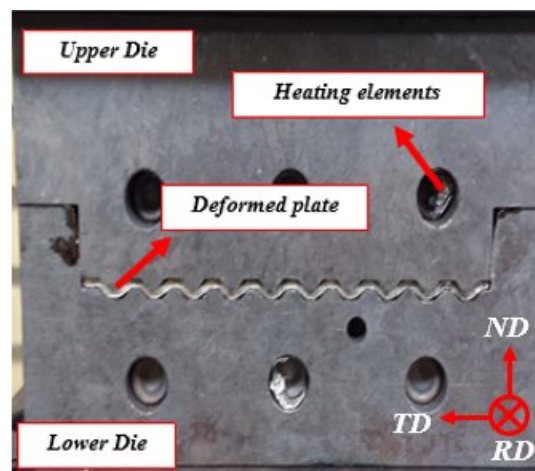


**Fig. 2**  
The CGP die set up with heating elements.

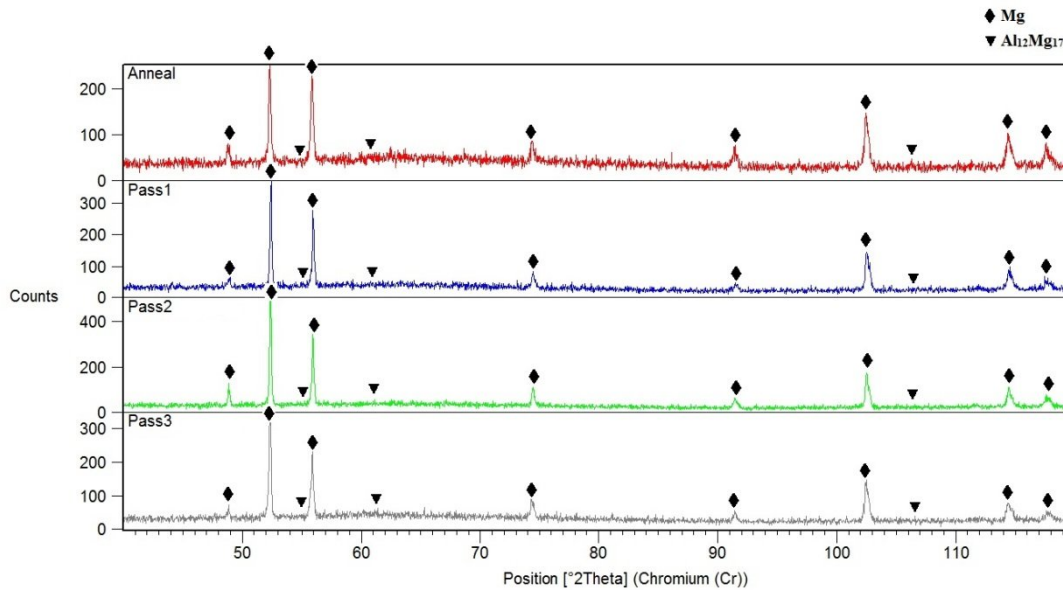
### 3 RESULTS AND DISCUSSION

#### 3.1 Microstructural and textural evolutions

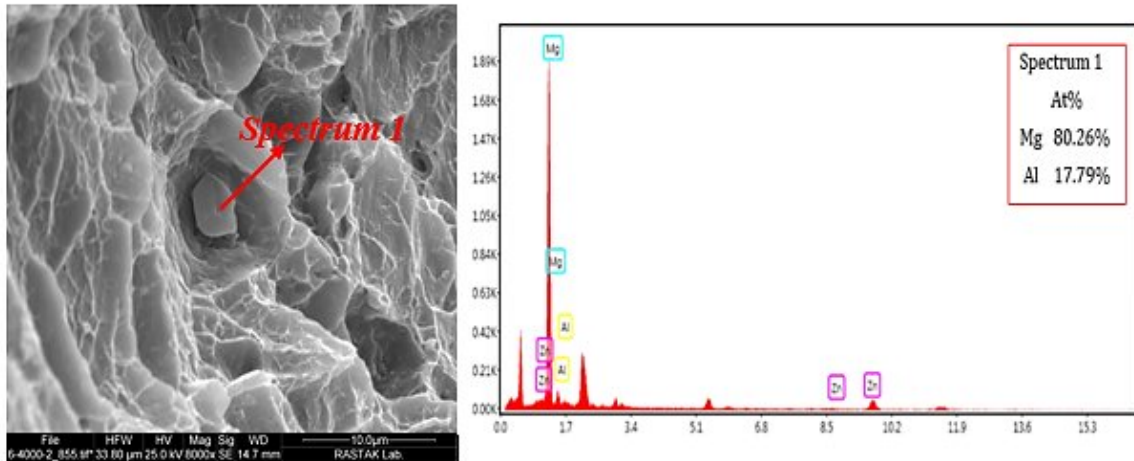
The XRD patterns for various samples are given in Fig. 3, indicating a short peak near  $2\theta=106^\circ$  that reveals the possibility of the second phase ( $Mg_{17}Al_{12}$ ) existence in the annealed sample of AZ91D Mg alloy. It means that the microstructure of the annealed specimen consists of certain volume fraction of  $\beta$ - $Mg_{17}Al_{12}$  intermetallic compounds, which are most likely divided among the grain boundaries.

The SEM micrograph and EDS spectrum of the fracture surface of the annealed AZ91D Mg alloy, shown in Fig. 4, can approve the existence of the  $\beta$ - $Mg_{17}Al_{12}$  particles in the microstructure of the annealed worksheet. As a result, it could be claimed that similar to the annealed sheet,  $\beta$ - $Mg_{17}Al_{12}$  particles might exist in various CGPed specimens. However, since the weight percentage of this phase was probably less than five, XRD patterns illustrated in Fig. 3 could not detect this intermetallic phase in various deformed parts.

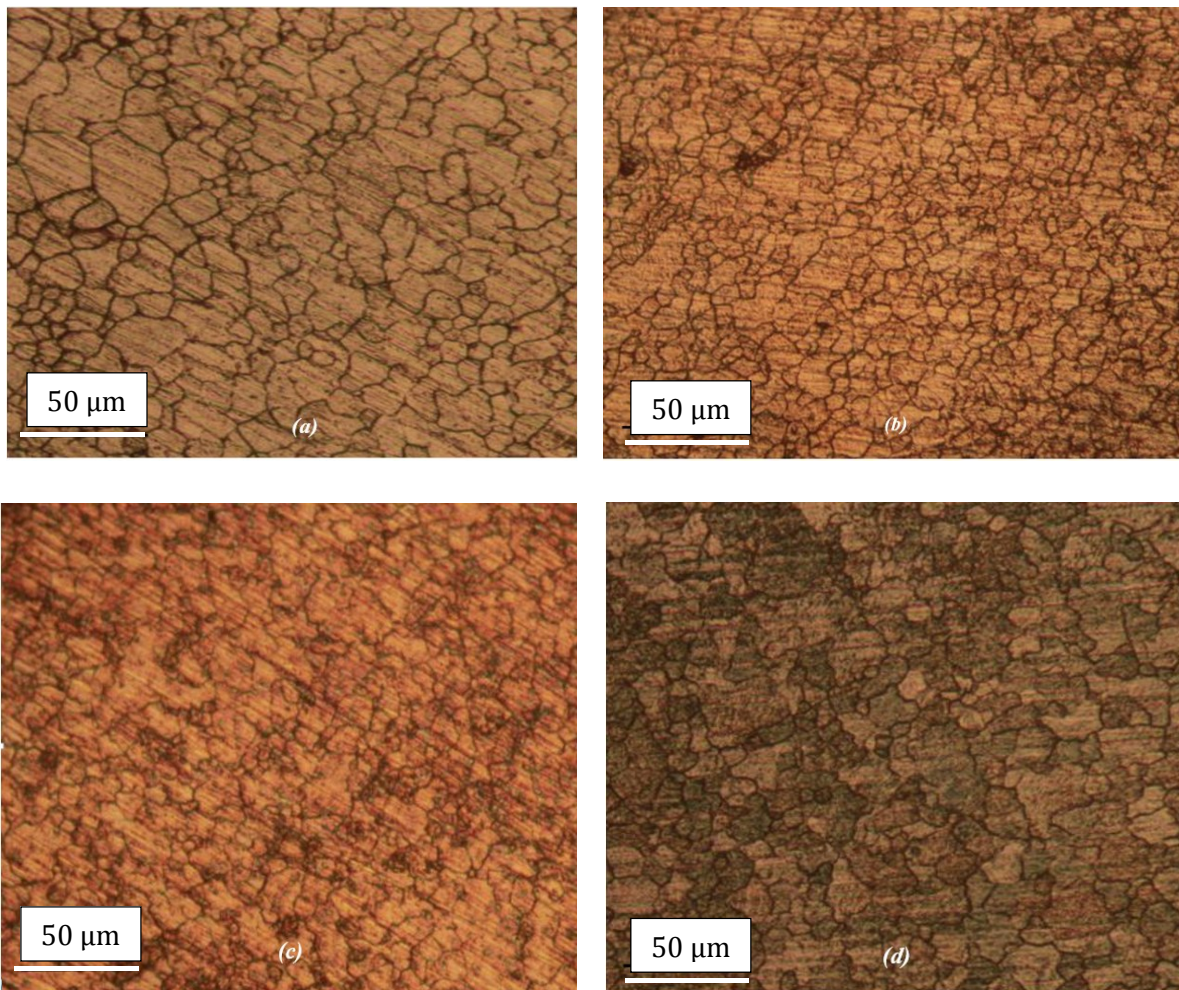
Fig. 5 illustrates the microstructure of the TD-ND section for the annealed sample and the sheets after one, two and three CGP cycles. As can be seen in Fig. 5, equiaxed grains can be observed in different cases. Moreover, there is not any sign of twinning in the microstructures of the CGPed specimens. This might mainly be due to long-time preheating stage for each CGP cycle.



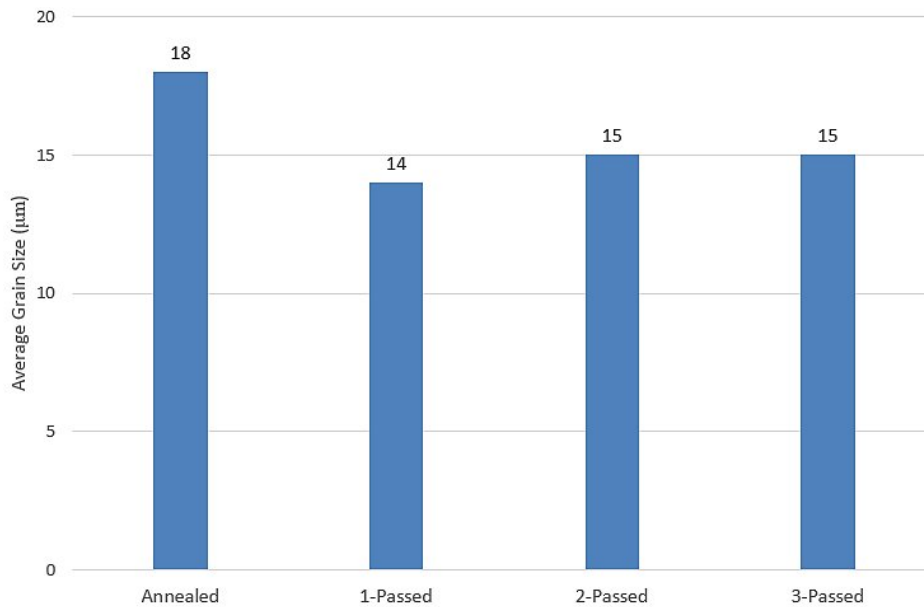
**Fig. 3**  
X-ray diffraction spectra for different samples of AZ91D Mg alloy.



**Fig. 4**  
SEM image of the annealed AZ91D Mg alloy (left) and the corresponding EDS analysis of the particle (right).



**Fig. 5**  
The microstructures of the annealed (a) AZ91D Mg alloy, together with the samples CGPed by one pass (b), two passes (c) and three passes (d).

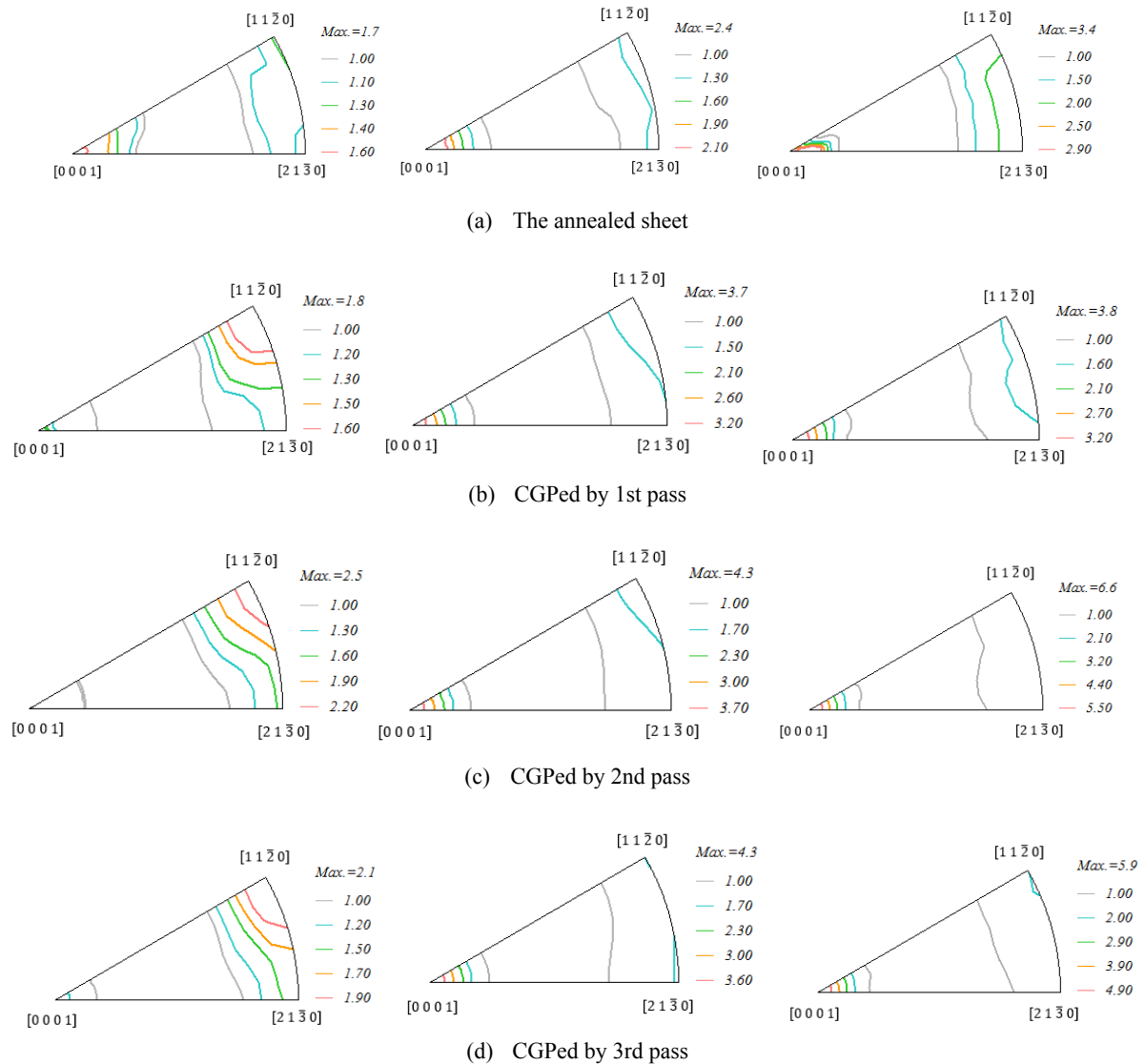


**Fig. 6**

The average grain sizes of the annealed and different CGPed specimens.

The average grain sizes (AGS) of various worksheets are plotted in Fig. 6. The annealed one has an average grain size of 18  $\mu\text{m}$ . After one pass, based on huge strain induction in CGP process, the AGS was reduced to 14  $\mu\text{m}$ . This is due to the mechanical work and elevated temperature effects on the microstructure, simultaneously. Performing the CGP process at an elevated temperature (300  $^{\circ}\text{C}$ ), where  $T > 0.5T_m$  (in Kelvin), and inducing large plastic strains resulted in dynamic recrystallization (DRX) in the material. The  $\beta\text{-Mg}_{17}\text{Al}_{12}$  particles in the 1-passed specimen were in a size range of greater than 1  $\mu\text{m}$  (see Fig. 4), where particle stimulated nucleation (PSN) would be expected [32]. Thus, the AGS decrease from the annealed sheet to 1-passed sample implies that the dynamic recrystallization (DRX) occurred based on the PSN mechanism. The grains next to the  $\beta\text{-Mg}_{17}\text{Al}_{12}$  particles were finer in comparison with the other grains. As can be seen in Figs. 5 (c) and (d), there was a little increase in AGS during the second and third passes of the forming process. It could be caused by minor grain growth during the preheating at 300  $^{\circ}\text{C}$  for each stage of a CGP cycle that might overcome the DRX grain refinement during the 2nd and 3rd passes. This result is in contrast with those of the previous researches for hot mechanical working of AZ91 Mg alloy [33-35]. The AGSes of the 2-passed and 3-passed samples are nearly the same and equal to 15  $\mu\text{m}$ .

Among various microstructural parameters affecting the mechanical properties of a material, the texture is the most important one for polycrystalline alloys. The  $\{0002\}$  and  $\{10\bar{1}0\}$  incomplete pole figures of the annealed and CGPed AZ91D sheets were used to obtain their inverse pole figures. These IPFs are shown in Fig. 7. The IPFs of the annealed sheet for RD, TD and ND can be observed in Fig. 7(a). The IPF of RD for this sample demonstrates the texture lines with an intensity of 1.7 multiples random distribution (MRD) concentrated on  $[0\ 0\ 0\ 1]$  direction that means  $[0\ 0\ 0\ 1]$  direction of many grains is parallel to the RD. The IPF of TD shows that the main texture is  $[0\ 0\ 0\ 1] \parallel \text{TD}$  with 2.4 MRD intensity. Finally, the IPF of ND indicates that there is a very strong  $[0\ 0\ 0\ 1] \parallel \text{ND}$  texture in the annealed AZ91D Mg alloy sheet by an intensity of 3.4 MRD. Therefore, it can be claimed that intensive basal texture existed in the annealed sheet. It is in contrast with Tolouie's report [36]. When the annealed worksheet was deformed via the first pass of the CGP process, the IPF of RD shows a change in the main texture from  $[0\ 0\ 0\ 1] \parallel \text{RD}$  to  $[1\ 1\ \bar{2}\ 0] \parallel \text{RD}$  with a maximum intensity of 1.8 MRD. Although the main texture of TD and ND IPFs for the 1-passed specimen does not vary from  $[0\ 0\ 0\ 1]$  direction, but the maximum intensities of these IPFs were increased to 3.7 and 3.8 MRD, respectively. Based on the ND IPF of the 1-passed specimen, one could conclude that the intensity of basal texture was not changed significantly (just about 10%). It means that the basal texture of AZ91D Mg sheet was controlled during 1-pass CGP process. It is in good agreement with the findings previously reported for different Mg alloys [37-40]. Although the main texture directions of 2-passed and 3-passed specimens did not vary, basal texture intensities of these two samples were out of control and increased significantly (even up to about 95%). This point is clear in Figs. 7(c) and (d), where the ND IPFs of 2-passed and 3-passed specimens are demonstrated.

**Fig. 7**

Inverse pole figures (IPFs) of different worksheets [RD (left), TD (middle), and ND (right)].

Fig. 8 shows the maximum texture intensity of  $[0\ 0\ 0\ 1]$  direction for the RD, TD and ND of various samples. The maximum intensity of RD IPF for  $[0\ 0\ 0\ 1]$  direction was reduced from 1.7 MRD for the annealed sample to about 1.3 MRD for the 1-passed specimen (see Figs. 7(a) and 7(b)). In other words, after the first pass, the number of grains that their  $[0\ 0\ 0\ 1]$  direction was parallel to the RD was reduced. This drop should reveal its effect by increasing the number of grains that their  $[0\ 0\ 0\ 1]$  direction was parallel to the TD and ND directions for the 1-passed sample. As can be seen in Fig. 7, the maximum intensities of TD and ND IPFs of 1-passed sheet for  $[0\ 0\ 0\ 1]$  direction have been enhanced from 2.4 and 3.4 MRD (for the annealed sample) to 3.7 and 3.8 MRD, respectively (see Figs. 7(a) and 7(b)). Therefore, after just one pass of CGP process, the number of grains that their  $[0\ 0\ 0\ 1]$  direction was parallel to TD and ND have been increased. However, the increase of these two sets of grains was controlled in such a way that basal texture has not been increased significantly. Moreover, by strengthening of texture component parallel to TD, the possibility of basal texture formation would be reduced [41]. Accordingly, based on Figs. 7 and 8, basal texture enhancement has been controlled in the 1-passed specimen. Controlling the

basal texture of AZ91D Mg alloy via performing the first CGP cycle could be introduced as an important achievement of the present investigation. Afterwards, by performing the subsequent CGP cycles, namely the second and third passes, the maximum intensities of RD IPFs for  $[0\ 0\ 0\ 1]$  direction reduced to 1.0 and 1.2 MRD, respectively.

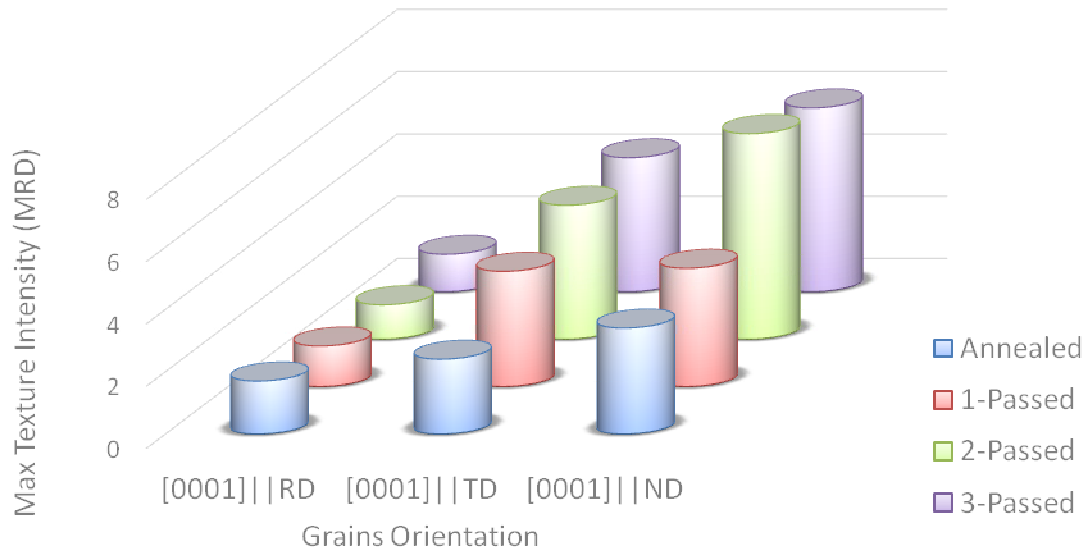


**Fig. 8**

Maximum texture intensity of  $[0\ 0\ 0\ 1]$  direction with respect to the RD, TD and ND for different worksheets.

As it has been stated previously, the out of control changes in basal texture of the 2-passed and 3-passed worksheets, has been due to the high texture intensities of ND IPFs for  $[0\ 0\ 0\ 1]$  direction for these two specimens. Fig. 7 shows that the maximum texture intensities in the ND IPFs for  $[0\ 0\ 0\ 1]$  direction for 2-passed and 3-passed samples are 6.6 MRD and 5.9 MRD, respectively. Hence, it could be claimed that after performing the second and third CGP cycles for AZ91D Mg alloy, the basal texture would be out of control and increased significantly.

As the last point in this section, it should be noted that the PSN mechanism develops random texture [42]. It is obvious from Figs. 7 and 8 that after the first CGP cycle and as more CGP passes (i.e. the 2nd and 3rd passes) are conducted on the AZ91D Mg sheet, the maximum texture intensity in all the IPFs for each individual direction has been enhanced. In other words, the probability of PSN-mechanism occurrence was more for the 1-passed specimen and less for the 2 and 3-passed samples. Therefore, it could be concluded that the  $\beta$ -Mg<sub>17</sub>Al<sub>12</sub> particles have been dissolved in the AZ91D Mg sheet during the second and third cycles of the CGP operation.

### 3.2 Mechanical properties

#### 3.2.1 Microhardness

Vickers Microhardness of the annealed sheet as well as various severe plastically deformed parts is demonstrated in Fig. 9. To discuss the hardness variation, two important variables, namely the average grain size (AGS) and the texture, should simultaneously be considered.

As it could be observed in Fig. 9, the annealed sheet has an average microhardness of about 80.8 H<sub>V</sub>. By inducing certain plastic strains during the first CGP cycle, the AGS of 1-passed specimen decreased in comparison with the annealed sheet. Therefore, based on the Hall-Petch relation, it was expected to observe an increase in the hardness of the specimen, namely to an average value of 86.3 H<sub>V</sub>. The Hall-Petch relation is presented in equation (1), where,  $\sigma_y$  is the yield strength,  $\sigma_i$  is the overall resistance of the lattice to dislocation movement,  $d$  is the average grain size, and  $k$  is a constant that related to the grain boundary locking term. However, after the second pass, a minor increase (about 1  $\mu\text{m}$ ) was observed in the AGS of the 2-passed Mg sheet. However, the average hardness of this workpiece was enhanced up to 92.5 H<sub>V</sub>. The only reason for the higher hardness of 2-passed sample compared with the 1-passed one is the crystallographic texture. It should be mentioned that the  $[1\ 1\ \bar{2}\ 0]$  direction is the most closed pack direction of the HCP structure. Therefore, it could be said that when the texture is such that the  $[1\ 1\ \bar{2}\ 0]$  direction is parallel to the axis of the indenter of the microhardness testing machine, a higher H<sub>V</sub> should be obtained. Based on Fig. 10, the texture intensities of  $[1\ 1\ \bar{2}\ 0] \parallel \text{RD}$  for the 1-passed and 2-passed specimens are 1.8 MRD and 2.5 MRD, respectively. This has led to a higher hardness for 2-passed sheet compared with the 1-passed one. Finally, the average hardness of the 3-passed workpiece was measured to be 79.2 H<sub>V</sub>. Since both the 2 and 3-passed samples represented the same average grain size of 15  $\mu\text{m}$ , the texture studies should be employed to interpret the difference between the microhardness of these specimens. With this regard, intensity reduction in the  $[1\ 1\ \bar{2}\ 0] \parallel \text{RD}$  texture component for the 3-passed sample compared with the 2-passed one (from 2.5 MRD to 2.1 MRD) is the most important reason for the lower microhardness of the former deformed sheet.

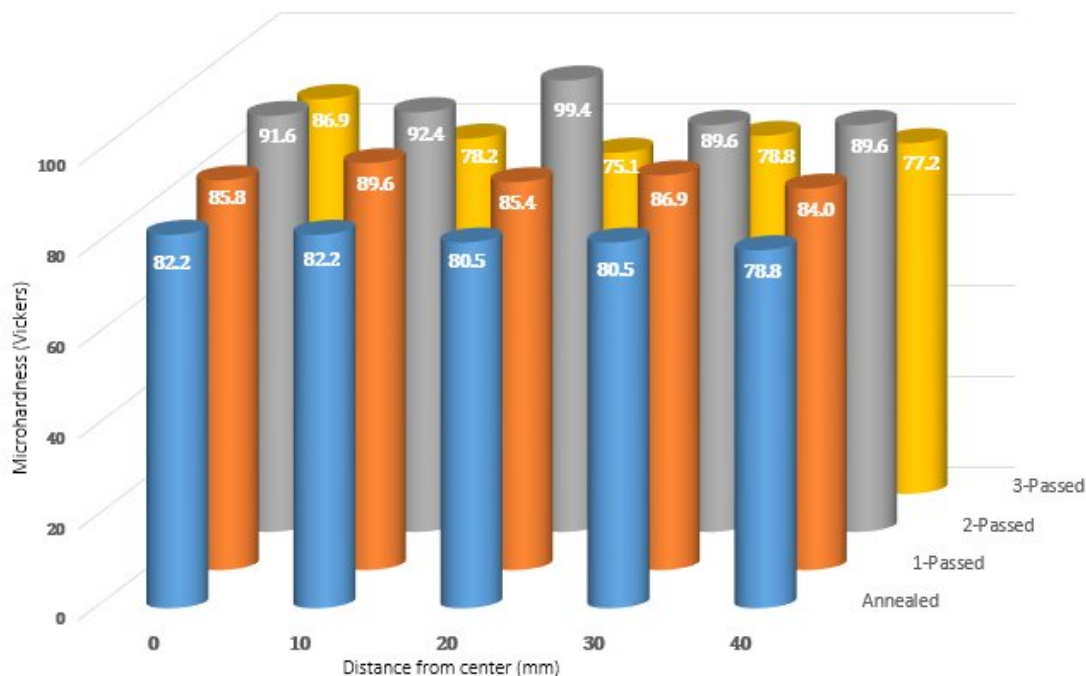


**Fig. 9**

The Vickers hardness of different samples versus the distance from the sheet center in TD-ND plane.

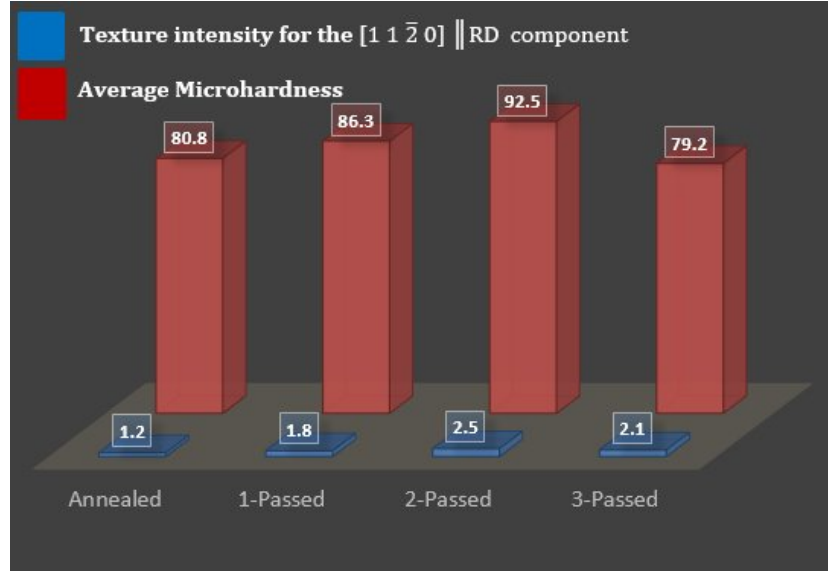


**Fig. 10**

The average microhardness and texture intensity for the  $[1\ 1\ \bar{2}\ 0] \parallel \text{RD}$  component of different samples.

$$\sigma_y = \sigma_i + kd^{-1/2} \quad (1)$$

To calculate the homogeneity of hardness distribution in various specimens, the inhomogeneity factor (IF) is determined by using the equations [2-3] [23]:

$$IF = \frac{\sqrt{\frac{1}{n-1} \sum_{i=1}^n (H_i - H_{ave})^2}}{H_{ave}} \times 100 \quad (2)$$

$$H_{ave} = \frac{1}{n} \sum_{i=1}^n H_i \quad (3)$$

In equation (1),  $H_i$  represents the microhardness of  $i$ -th measurement at a specific distance from the center of TD-ND section of the sheet,  $n$  shows the number of microhardness measurements for each worksheet and  $H_{ave}$  is the average microhardness. It can be claimed that, more homogeneity of the microstructure and material is a consequence of a smaller IF. The IF of each worksheet is illustrated in Fig. 11. As it can be seen in this figure, the annealed sheet has the minimum IF value, specifically 1.76. It means that the annealed sheet represents the highest homogeneity. As different CGP cycles are performed, the IF values of the deformed worksheets are gradually increased. Inducing greater severe plastic strains during each CGP pass and the texture evolution, discussed above comprehensively, are the main reasons for IF increasing through the subsequent cycles of the CGP operation. Hence, the 3-passed specimen possesses the maximum IF value and lowest homogeneity.

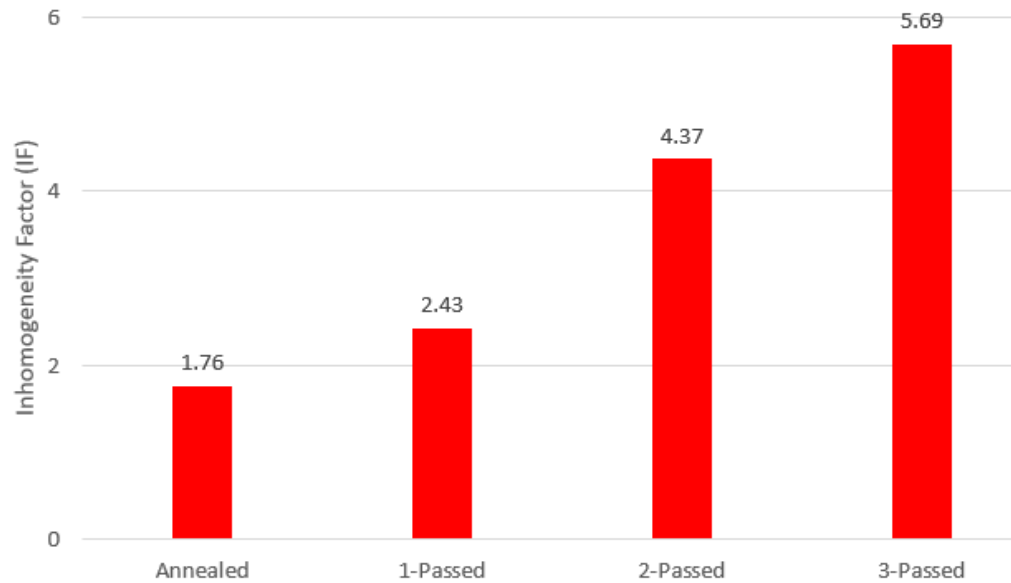


**Fig. 11**

The inhomogeneity factor (IF) of the annealed and different deformed AZ91D samples.

### 3.2.2 Tensile test results

The stress-strain curves of the annealed and CGPed workpieces in RD are illustrated in Fig. 12. Moreover, the mechanical properties of different specimens are shown in Table 1. As it can be found in Fig. 12 and Table 1, the yield strength (YS) and ultimate tensile strength (UTS) of the annealed sheet increased from 129.4 and 245.7 MPa to 166.7 and 261.1 MPa, respectively, after just the 1st pass of the CGP operation. These enhancements, namely 29% for YS and 7% for UTS, were mainly due to the grain refinement of the worksheet during the first CGP cycle (see Fig. 6). This observation is in good agreement with the Hall-Petch relation. As a result, it can be said that the grain refinement during the first cycle of the operation had a significant effect on YS improvement. The YS and UTS of the 2-passed sample, to be precise 135.9 and 246.0 MPa, respectively decreased by about 19% and 6% in comparison with those of the 1-passed specimen. Finally, for the worksheet subjected to three cycles of the CGP process, the YS and UTS significantly reduced to 96.3 and 207.1 MPa, respectively; even less than those of the annealed sheet! The elongations of the annealed sheet as well as workpieces CGPed through one, two and three passes were also 24.5%, 36.1%, 24.7% and 18.5%, respectively. An elongation enhancement of 48% by performing just the first pass of CGP operation is another important and surprising achievement of the present study. Nevertheless, during the second CGP cycle, by 32% drop in the elongation its value reduced almost to that of the annealed specimen. This situation continued to the third cycle of the operation and the 3-passed sheet has exhibited the lowest elongation, namely 18.5%, among various deformed and undeformed samples.

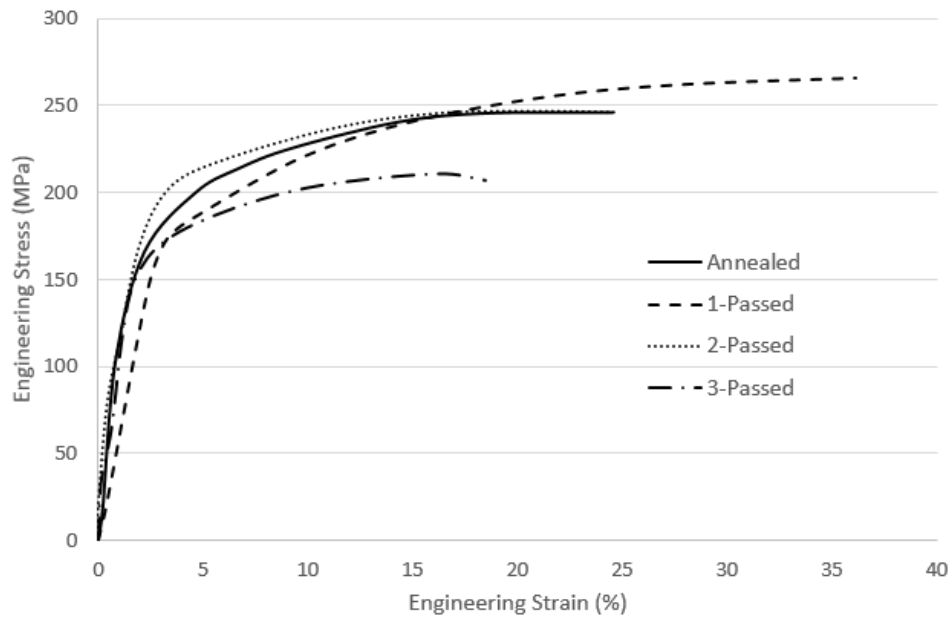


**Fig. 12**  
The engineering stress-strain curves of different AZ91D Mg alloy samples.

**Table 1**  
Mechanical properties of the annealed and various CGPed specimens in RD.

Sample	Yield Strength (MPa)	Ultimate Tensile Strength (MPa)	Elongation (%)
Annealed	<b>129.4</b>	<b>245.7</b>	<b>24.5</b>
1-Passed	<b>166.7</b>	<b>261.1</b>	<b>36.1</b>
2-Passed	<b>135.9</b>	<b>246.0</b>	<b>24.7</b>
3-Passed	<b>96.3</b>	<b>207.1</b>	<b>18.5</b>

In addition to microstructure and AGS, the texture is an important factor causing changes in mechanical properties of a plastically deformed component. As discussed previously, in the annealed specimen, there was predominantly a basal texture. By performing the first CGP cycle, the basal texture intensity in the 1-passed specimen was controlled. It means that the texture intensity of the 1-passed specimen has not increased significantly (see section 3.1 and Fig. 8). Therefore, for the 1-passed sample, by controlling the basal texture or preventing the formation of a stronger basal texture, during the subsequent tensile test, the dislocations could pass more intervals inside the grains, resulting in a higher ductility [28]. The minor grain growth and probably the reduction in amount of  $\beta$ -Mg<sub>17</sub>Al<sub>12</sub> phase (see Fig. 3), due to the sample long-time preheating to the target temperature, could subsequently decrease the YS and UTS of the 2-passed sheet in comparison with the 1-passed part. Moreover, increase in the basal texture intensity of the 2-passed specimen in the ND IPF (see Fig. 7) is the main reason for reduction in elongation of the 2-passed sample in comparison with the 1-passed one. The same reasoning could be expressed to justify the variations in mechanical properties of the AZ91D sample subjected to three cycles of the CGP operation.

## 4 CONCLUSIONS

In this research, the evolution of the microstructure, texture and mechanical properties of AZ91D Mg alloy annealed sheets during three cycles of the constrained groove pressing have been investigated. Based on the findings presented and discussed in this article, the important conclusions can be summarized as below:

1. AGS reduction is observed from the annealed sheet (18 $\mu$ m) to 1-passed sample (14 $\mu$ m), implying that dynamic recrystallization (DRX) has occurred based on PSN mechanism due to existence of  $\beta$ -Mg<sub>17</sub>Al<sub>12</sub> particles. The grain growth according to preheating up to 300 °C for each stage of a CGP cycle, has almost overcome the DRX during the 2nd and 3rd passes of the process. This situation provided microstructures with an AGS of about 15 $\mu$ m after the 2nd and 3rd CGP cycles.
2. The basal texture of the annealed AZ91D Mg alloy sheet was controlled by performing just the first CGP cycle and the texture component parallel to TD found more intensity in the 1-passed sample.
3. With increasing the induced plastic strain and certain texture evolutions during the subsequent CGP cycles, the homogeneity of the sheet reduced such that the lowest homogeneity, with the maximum IF of 5.69, was represented by the 3-pass CGPed sample.
4. After the 1st CGP cycle, 28.8%, 6.3% and 47.3% improvements in YS, UTS and elongation were respectively observed, as a result of basal texture controlling in the sample. However, by continuing the process through the subsequent cycles, these mechanical properties were considerably reduced.

## REFERENCES

- [1] Kojima Y. Handbook advanced Mg technology. Tokyo: Kallos Publishing Co.; 2000.
- [2] Ferdowsi, M.R.G., Mazinani, M. and Ebrahimi, G.R., 2014. Effects of hot rolling and inter-stage annealing on the microstructure and texture evolution in a partially homogenized AZ91 magnesium alloy. *Materials Science and Engineering: A*, 606, pp.214-227.
- [3] Azzeddine, H., Abdessameud, S., Alili, B., Boumerzoug, Z. and Bradai, D., 2011. Effect of grain boundary misorientation on discontinuous precipitation in an AZ91 alloy. *Bulletin of Materials Science*, 34(7), pp.1471-1476.
- [4] Huang, X., Suzuki, K., Chino, Y. and Mabuchi, M., 2015. Texture and stretch formability of AZ61 and AM60 magnesium alloy sheets processed by high-temperature rolling. *Journal of Alloys and Compounds*, 632, pp.94-102.
- [5] Guo, L. and Fujita, F., 2015. Influence of rolling parameters on dynamically recrystallized microstructures in AZ31 magnesium alloy sheets. *Journal of Magnesium and Alloys*, 3(2), pp.95-105.
- [6] Ebrahimi, G.R., Maldar, A.R., Ebrahimi, R. and Davoodi, A., 2010. The effect of homogenization on microstructure and hot ductility behaviour of AZ91 magnesium alloy. *Kovove Mater*, 48, pp.277-284.
- [7] Valiev, R.Z., Korznikov, A.V., Mulyukov, R.R. 1993. Structure and Properties of Ultrafine-grained Materials Produced by Severe Plastic Deformation. *Materials Science and Engineering A* 168(2):141–148.
- [8] Rosochowski, A. 2005. Processing Metals by Severe Plastic Deformation. *Solid State Phenomena* 101–102:13–22.
- [9] Shin, D.H., Park, J.J., Kim, Y.S., Park, K.T. 2002. Constrained groove pressing and its application to grain refinement of aluminum. *Materials Science and Engineering A328*. 98–103.
- [10] Lee, J.W., Park, J.J. 2002. Numerical and experimental investigations of constrained groove pressing and rolling for grain refinement. *Journal of Materials Processing Technology* 130–131. 208–213.
- [11] Rafizadeh, E., A. Mani, and M. Kazeminezhad. 2009. The effects of intermediate and post-annealing phenomena on the mechanical properties and microstructure of constrained groove pressed copper sheet. *Materials Science and Engineering: A*. 515(1-2): p. 162-168.
- [12] Sathesh Kumar, S.S., Raghu, T. 2013. Mechanical behaviour and microstructural evolution of constrained groove pressed nickel sheets. *Journal of Materials Processing Technology* 213. 214–220.
- [13] Fong, K.S., Tan, M.J., Chua, B.W., Atsushi, D. 2015. Enabling wider use of Magnesium Alloys for lightweight applications by improving the formability by Groove Pressing. *Procedia CIRP* 26. 449 – 454.
- [14] Hajizadeh, K., Ejtemaei, S. and Eghbali, B., 2017. Microstructure, hardness homogeneity, and tensile properties of 1050 aluminum processed by constrained groove pressing. *Applied Physics A*, 123(8), p.504.
- [15] Lin, P., Tang, T., Zhao, Z., Wang, W. and Chi, C., 2017. Refinement Strengthening of AZ31 Magnesium Alloy by Warm Constrained Groove Pressing. *Materials Science*, 23(1), pp.84-88.

- [16] Pouraliakbar, H., Jandaghi, M.R. and Khalaj, G., 2017. Constrained groove pressing and subsequent annealing of Al-Mn-Si alloy: microstructure evolutions, crystallographic transformations, mechanical properties, electrical conductivity and corrosion resistance. *Materials & Design*, 124, pp.34-46.
- [17] Moradpour, M., Khodabakhshi, F., Mohebbpour, S.R., Eskandari, H. and Haghshenas, M., 2019. Finite element modeling and experimental validation of CGP classical and new cross routes for severe plastic deformation of an Al-Mg alloy. *Journal of Manufacturing Processes*, 37, pp.348-361.
- [18] Nazari, F., Honarpisheh, M. and Zhao, H., 2019. Effect of stress relief annealing on microstructure, mechanical properties, and residual stress of a copper sheet in the constrained groove pressing process. *The International Journal of Advanced Manufacturing Technology*, 102(9-12), pp.4361-4370.
- [19] Mozafari, J., Khodabakhshi, F., Eskandari, H. and Haghshenas, M., 2019. Wear Resistance and Tribological Features of Ultra-Fine-Grained Al-Mg Alloys Processed by Constrained Groove Pressing-Cross Route. *Journal of Materials Engineering and Performance*, 28(2), pp.1235-1252.
- [20] Hoseini-Athar, M.M., Mahmudi, R., Babu, R.P. and Hedström, P., 2019. Microstructural evolution and superplastic behavior of a fine-grained Mg-Gd alloy processed by constrained groove pressing. *Materials Science and Engineering: A*, 754, pp.390-399.
- [21] Wang, Z., Wang, T., Guan, Y., Wei, X., Fang, X., Zhu, G. and Gao, S., 2019. Effects of lubrication and strain path on constrained groove pressing of commercially pure aluminum sheets. *The International Journal of Advanced Manufacturing Technology*, pp.1-17.
- [22] Ghorbanhosseini, S. and Fereshteh-saniee, F., 2019. Multi-objective optimization of geometrical parameters for constrained groove pressing of aluminium sheet using a neural network and the genetic algorithm. *Journal of Computational Applied Mechanics*, 50(2), pp.275-281.
- [23] Ghorbanhosseini, S., Fereshteh-Saniee, F. and Sonboli, A., 2020. Development of new fiber textures for enhancing mechanical properties of 2024 Al alloy using elevated-temperature constrained groove pressing. *Materials Science and Engineering: A*, 796, p.140210.
- [24] Karademir, I., Celik, M.B., Husem, F., Maleki, E., Amanov, A. and Unal, O., 2021. Effects of constrained groove pressing, severe shot peening and ultrasonic nanocrystal surface modification on microstructure and mechanical behavior of S500MC high strength low alloy automotive steel. *Applied Surface Science*, 538, p.147935.
- [25] Keyvani, A., Naseri, M., Imantalab, O., Gholami, D., Babaei, K. and Fattah-alhosseini, A., 2021. Microstructural characterization and electrochemical behavior of nano/ultrafine grained pure copper through constrained groove pressing (CGP). *Journal of Materials Research and Technology*, 11, pp.1918-1931.
- [26] Bhardwaj, A., Gohil, N., Gupta, A.K. and Kumar, S.S., 2021. An experimental investigation on the influence of elevated-temperature constrained groove pressing on the microstructure, mechanical properties and hardening behaviour of Ti6Al4V alloy. *Materials Science and Engineering: A*, 802, p.140651.
- [27] Wang, Z., Wang, T., Guan, Y. and Zhu, L., 2021. Effect of strain path on microstructure and mechanical properties of AZ31 magnesium alloy sheets processed by constrained groove pressing. *Materials Science and Engineering: A*, 804, p.140794.
- [28] Nazari, F., Honarpisheh, M. and Zhao, H., 2021. Effect of the uncertainty of multi-cut contour method and friction coefficient on residual stresses of constrained groove pressing process. *Proceedings of the Institution of Mechanical Engineers, Part C: Journal of Mechanical Engineering Science*, p.0954406220948908.
- [29] Fereshteh-Saniee, F., Ghorbanhosseini, S. and Yaghoubi, S., 2021. A comprehensive comparison between the effect of elevated temperature constrained groove pressing on the microstructural evolutions, crystallographic texture, and mechanical properties of Al 2024 and Mg AZ91D alloys. *Proceedings of the Institution of Mechanical Engineers, Part E: Journal of Process Mechanical Engineering*, p.095440892111043603.
- [30] ASTM E3-11, C., 2017. ASTM standards. Philadelphia: American Society for Testing Materials.
- [31] Xing, J., Yang, X., Miura, H. and Sakai, T., 2008. Mechanical properties of magnesium alloy AZ31 after severe plastic deformation. *Materials Transactions*, 49(1), pp.69-75.
- [32] Callister, W.D., 2000. *Fundamentals of materials science and engineering*. Wiley.
- [33] Mao, L., Liu, C., Gao, Y., Han, X., Jiang, S. and Chen, Z., 2017. Microstructure and mechanical anisotropy of the hot rolled Mg-8.1 Al-0.7 Zn-0.15 Ag alloy. *Materials Science and Engineering: A*, 701, pp.7-15.
- [34] Alili, B., Azzeddine, H., Abib, K. and Bradai, D., 2013. Texture evolution in AZ91 alloy after hot rolling and annealing. *Transactions of Nonferrous Metals Society of China*, 23(8), pp.2215-2221.
- [35] Guo, F., Zhang, D., Wu, H., Jiang, L. and Pan, F., 2017. The role of Al content on deformation behavior and related texture evolution during hot rolling of Mg-Al-Zn alloys. *Journal of Alloys and Compounds*, 695, pp.396-403.
- [36] Tlouie, E. and Jamaati, R., 2018. Effect of  $\beta$ -Mg<sub>17</sub>Al<sub>12</sub> phase on microstructure, texture and mechanical properties of AZ91 alloy processed by asymmetric hot rolling. *Materials Science and Engineering: A*, 738, pp.81-89.
- [37] Mukai, T., Yamanoi, M., Watanabe, H. and Higashi, K., 2001. Ductility enhancement in AZ31 magnesium alloy by controlling its grain structure. *Scripta materialia*, 45(1), pp.89-94.
- [38] Kim, W.J., Hong, S.I., Kim, Y.S., Min, S.H., Jeong, H.T. and Lee, J.D., 2003. Texture development and its effect on mechanical properties of an AZ61 Mg alloy fabricated by equal channel angular pressing. *Acta materialia*, 51(11), pp.3293-3307.
- [39] Agnew, S.R., Horton, J.A., Lillo, T.M. and Brown, D.W., 2004. Enhanced ductility in strongly textured magnesium produced by equal channel angular processing. *Scripta Materialia*, 50(3), pp.377-381.
- [40] Kim, W.J., An, C.W., Kim, Y.S. and Hong, S.I., 2002. Mechanical properties and microstructures of an AZ61 Mg Alloy produced by equal channel angular pressing. *Scripta materialia*, 47(1), pp.39-44.

- [41] Randle, V. and Engler, O., 2014. Introduction to texture analysis: macrotexture, microtexture and orientation mapping. CRC press.
- [42] Humphreys, F.J. and Hatherly, M., 2012. Recrystallization and related annealing phenomena. Elsevier.
- [43] Fereshteh-Saniee, F., Ghorbanhosseini, S. and Yaghoubi, S., 2024. A profound study of damage behavior for Al 2024-T3 alloy worksheet produced by constrained groove pressing in the superior practical condition. Scientific Reports, 14(1), p.17798.
- [44] Bhardwaj, A., Gohil, N., Sharma, A., Gupta, A.K. and Kumar, S.S., 2024. Microtexture and mechanical properties evolution of Ti6Al4V with varying pressing speeds of constrained groove pressing. Materials Today Communications, 38, p.108340.
- [45] Sawalkar, S. and Field, D.P., 2024. Constrained groove uniform pressing process for achieving homogeneously improved properties in copper. Materials Science and Engineering: A, 899, p.146417.
- [46] Farajollahi, M., Ebrahimi, M. and Ajori, S., 2024. Improving Wear Behavior of 304L Stainless Steel under Constrained Groove Pressing. Aerospace Mechanics, 20(2), pp.17-28.